ACS APPLIED MATERIALS & INTERFACES

Research Article

www.acsami.org

Why Condensate Drops Can Spontaneously Move Away on Some Superhydrophobic Surfaces but Not on Others

Jie Feng,*[,†,‡] Yichuan Pang,[‡] Zhaoqian Qin,[‡] Ruiyuan Ma,[†] and Shuhuai Yao*[,†]

[†]Department of Mechanical Engineering, The Hong Kong University of Science and Technology, Hong Kong, 999077, China

[‡]Department of Materials Science & Engineering, Zhejiang University of Technology, Hangzhou, 310014, China

Supporting Information

ABSTRACT: The coalesce-induced condensate drop motion on some superhydrophobic surfaces (SHSs) has attracted increasing attention because of its wide potential applications. However, microscopic mechanism of spontaneous motion has not been discussed thoroughly. In this study, we fabricated two types of superhydrophobic copper surfaces with sisal-like nanoribbon structures and defoliation-like nanosheet structures by different wet chemical oxidation process and followed by same fluorization treatment. With lotus leaf and butterfly wing as control samples, the spontaneous motion phenomenon of condensate drops on these four kinds of SHSs was investigated by using optical microscope under ambient conditions. The results showed that among all four types of SHSs, only superhydrophobic copper surfaces with sisal-like nanoribbon structures showed obvious spontaneous motion of condensate drops, especially when the relative humidity was higher. The microscopic mechanism of spontaneous motion was discussed in relation to the states of condensate drops on different nanostructures. It shows that the instantaneous Cassie state of condensed droplets prior to coalescence plays a key role in determining whether the coalesced drop departs, whereas only SHS possessing nanostructures with small enough Wenzel roughness parameter r (at least <2.1) and nanogaps forming high enough Laplace pressure favors the formation of the instantaneous Cassie state by completing the Wenzel−Cassie transition.

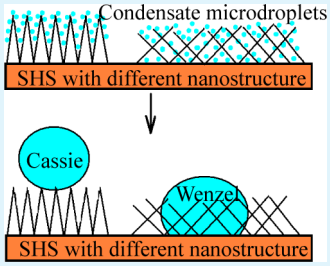

KEYWORDS: *superhydrophobic surface, condensate drop, spontaneous motion, microscopic mechanism, Wenzel roughness parameter, Wenzel−Cassie transition*

1. INTRODUCTION

The coalesce-induced condensate drop spontaneous motion on some superhydrophobic surfaces (SHSs)[1−5] has attracted increasing attention because of its potential applications in sustained dropwise condensation,[1,4,6−8] water collection,[9,10] anti-icing,[11,12] and anticorrosion.[13,14] However, microscopic mechanism of spontaneous motion of condensate drops, e.g., which type of SHSs support such spontaneous motion phenomena on them, has not been discussed thoroughly. For example, Liu et al[15] theoretically studied the mechanism of condensed drop jumping on SHSs and conclude that coalesced drop is in a metastable state with a driving force to reduce its base radius toward equilibrium state. Only after the coalescence of two or more small Cassie-state drops on a textured surface, can the merged composite drop easily transform to a 0 mm base radius and jump. However, their conclusion lacks experimental support. Jiang et al[16] correlated the work of adhesion of the surface to condensed water and self-removal efficiency and find that only microdroplets with near diameters can be self-removed after coalescing. However, they did not provide a clear answer to what kind of nanostructures indeed facilitate the spontaneous motion of condensate drops.

Rykaczewski et al[17,18] studied microdroplet growth mechanism during vapor condensation on SHSs by ESEM imaging and find that nucleating nanodroplets coalesce to create a wetted flat spot with a diameter of a few micrometers from which the microdroplet emerges and grows in purely constant base mode until reaching a contact angle of 130−150°. The key role of the nanoscale topography is confinement of the base area of forming droplets, which allows droplets to grow only through contact angle increase. The nearly spherical droplets formed in this fashion become highly mobile after coalescence. Wang et al[19] presented a mechanistic framework to explain the complex nature of water condensation on structured surfaces, which defines local energy barriers as key to understanding the growth process and identifies the role of nucleation density on the emergent droplet morphology. However, both their works seem too abstruse. The structural parameters and local energy barriers used in their explanations seem more like a special case of Laplace pressure principle.

In the present work, we fabricated two types of superhydrophobic copper surfaces with sisal-like nanoribbon structures and defoliation-like nanosheet structures by different wet chemical oxidation process[20−23] and followed by same fluorization treatment. Then we performed vapor condensation experiments on them. The control surfaces were lotus leaf and butterfly wing, two classical natural SHSs. The results showed that among all four types of SHSs, only superhydrophobic copper surfaces with sisal-like nanoribbon structures showed obvious spontaneous motion phenomenon of condensate

Received: August 23, 2012
Accepted: November 16, 2012
Published: November 16, 2012

   dx.doi.org/10.1021/am301767k | ACS Appl. Mater. Interfaces 2012, 4, 6618−6625

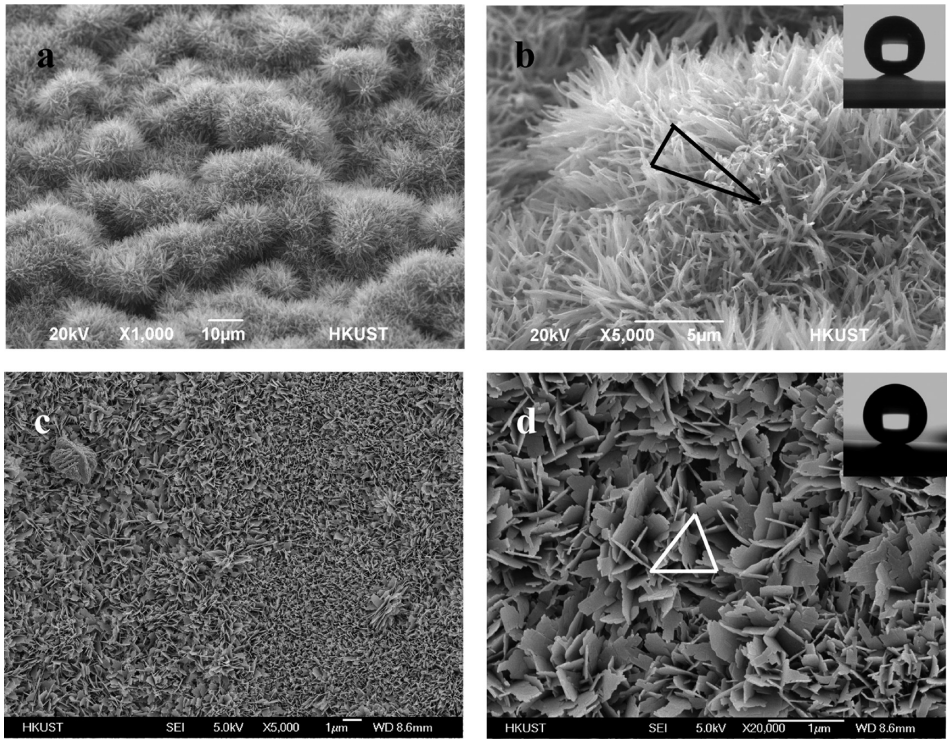

Figure 1. SEM images of (a, b) CuO sisal-like nanoribbon and(c, d) defoliation-like nanosheet structures on copper surfaces. Images b and d are magnified versions of a and c, respectively. The insets were profiles of 0.5−1 μL water drops on copper surfaces showing WCA at (b) 167.5 and (d) 161.5°, respectively.

drops, especially when the relative humidity (RH) was high. The microscopic mechanism of spontaneous motion phenomenon was discussed in a more straightforward way. We find that instantaneous Cassie state of condensed droplets prior to coalescence plays a key role in deciding whether the spontaneous motion occurs or not. The narrow and open nanogaps are favorable for the condensate droplets to retain at the Cassie state.

2. EXPERIMENTAL SECTION

Preparation. The copper foils with size of 10 cm × 10 cm × 0.5 mm (purity 99.99%, Aldrich) were first microroughened by immersing in an ultrasonic aqueous bath consisting of 100 g/L Iron(III) chloride ($FeCl_3$, anhydrous, 98%, VWR International Ltd., England) and 80 g/L hydrogen chloride (HCl, 37%, Scharlau) at room temperature for 10 min. After being rinsed by deionized water, these foils were incubated in diluted ammonia aqueous solution ($NH_3{\cdot}H_2O$, 28%, VWR International Ltd.) (0.03 M) at ∼5 °C for 96 h to make the surface form nanoribbon structures.[20,21] Then these blue foils were thoroughly washed with deionized water and dried at 180 °C for 2 h to make the $Cu(OH)_2$ become into stable CuO by completing dehydration reaction. Afterward, the black copper foils were incubated in a 0.5 wt % hexane solution of 1H,1H,2H,2H-perfluorodecyltriethoxysilane (FAS17, Sigma) at room temperature for 1 h, followed by drying at 110 °C for 1 h. For superhydrophobic copper surfaces with nanosheet structures, the copper foils were first immersed in 4 M HCl aqueous solution for 5 s to remove surface oxide and then ultrasonically washed in deionized water. After that, the copper foils were incubated in an aqueous solution of 2.5 M KOH and 0.065 M $K_2S_2O_8$ at 60 °C for 1 h while the residue procedures were same as above.[22,23]

Characterization. The morphology of the resulted copper surfaces was characterized by scanning electron microscopy (SEM, JEOL 6300). The water contact angles (CAs) and slide angles (SAs) of the final copper surfaces were measured by using a Dataphysics OCA35 contact-angle system with a temperature control stage. This stage can precisely maintain the temperature of SHS from −30 to 160 °C. The stability of superhydrophobicity of the copper surface under dew condensation was checked by measuring static CAs of 4 μL sessile water drops placed on the surface at different cooling stage or recording the dynamic changes of CAs of each 4 μL sessile droplet during the whole 10 min cooling procedure at different ambient RH.[5] The static CAs were measured and averaged over six measurements.

Condensation Experiments. Condensation experiments were performed in a closed room with area of 25 m^2 and height of 3 m. The ambient temperature was controlled at 25 °C and the RH was adjusted at 30, 60, and 90%. The superhydrophobic copper foils with size of 3 cm × 3 cm ×0.5 mm were placed on a horizontal aluminum block that was almost completely immersed in mixture of ice and water (holding the temperature at 0−1 °C). This ensured the copper foils stable thus the following video could be focused on the same area. The spontaneous motion of condensate drops was observed and visualized by an optical microscope (Nikon LV150) with a 10 × objective and a charge-coupled device camera at 25 fps. Spontaneous motion phenomenon was quantified by analyzing a 2 min representative video. Five short periods of time (only 1 s), e.g., at 0 s, 30 s, 60 s, 90 and 120 s were selected for statistic. All together 5 × 25 pieces of snapshots were used to quantify the average numbers of distinguishable drop location changes (emergence or disappear in sequential microscopic images) in 1 s video (here named as "spontaneous motion frequency").[5] For comparison, lotus leaf and butterfly wing were also used as substrate surfaces in the same above condensation experiments.

3. RESULTS AND DISCUSSION

3.1. Morphology and Superhydrophobicity of As-Fabricated Surfaces. Different with vertical CuO nanoribbons on flat copper surface fabricated by Yang et al[20] and Jiang et al,[21] herein our nanoribbons clusters seemed more like sisals (Figure 1a). This was caused by the early microroughening of copper surface brought by $FeCl_3$ etching. The nanoribbons with ∼5 μm length and ∼200 nm diameter perpendicularly grew out from the curve surface of the microstructures. As a

dx.doi.org/10.1021/am301767k | ACS Appl. Mater. Interfaces 2012, 4, 6618−6625

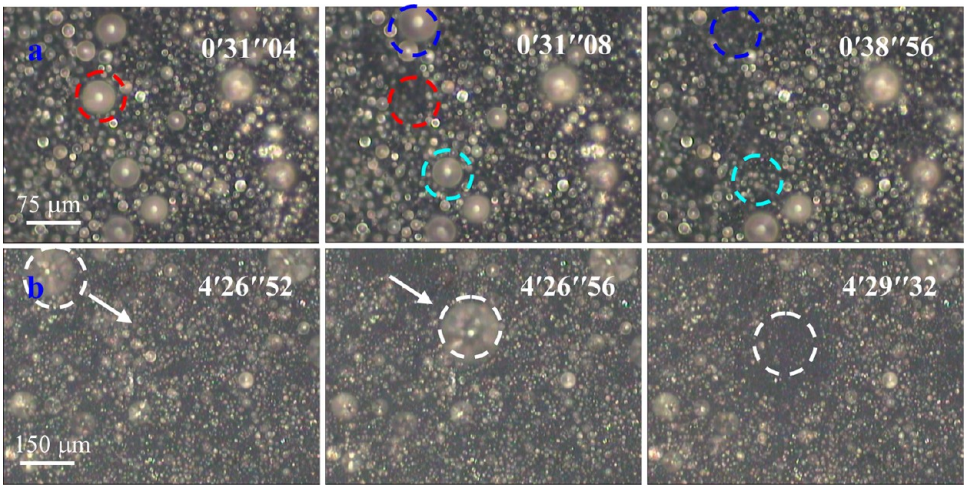

Figure 2. Time-lapse optical images (top-view) of dropwise condensation on horizontally placed superhydrophobic copper surface with sisal-like nanoribbon structures. The temperature of sample surface was 0−1 °C and the environmental RH was 90% (25 °C). The spontaneous motion frequency of condensed drops was as high as 72 drops/s (a) and the velocity was approximately 11.25 mm/s (b). Video S1 and S2 are available in the Supporting Information.

result, hierarchical structures similar with those of lotus leaf surface were fabricated. Figure 1b showed the defoliation-like nanosheet structures fabricated by directly oxidizing smooth copper surface with aqueous solution of KOH and $K_2S_2O_8$. It can be seen that although the nanosheets seemed much smaller in thickness (<50 nm) and even length (<1 μm) than the nanoribbons shown in Figure 1a, their perpendicularity was very poor. Similar structure has also been reported by Zhang et al.[22]

The superhydrophobic properties of the as-prepared surfaces were confirmed by measuring water CAs and SAs. According to the study by Zhang et al,[24] the smaller placed sessile droplets, the higher contact angles would be. Thus we splashed a very small drop (~0.5−1 μL) on the as-measured surfaces by using a polyethylene (PE) bottle with fine nozzle, then captured its profile and finally calculated the corresponding contact angle. The results showed that the CAs of the as-prepared copper surfaces with sisal-like nanoribbons and defoliation-like nanosheets were 167.5 ± 0.8° and 161.5 ± 1.2°, respectively. Both their SAs were 2°. However, when the measured drop volume was changed into 4 μL, the CAs were both less than 155°. The corresponding advancing and receding CAs of SHS with sisal-like nanoribbon structures were 156.1 ± 2.2 and 153.3 ± 3.3, respectively. The advancing and receding CAs of SHS with defoliation-like nanosheet structures were 156.0 ± 2.5 and 149.3 ± 1.2, respectively. This confirms that the as-prepared surfaces are typical superhydrophobic. The sufficiently low surface solid/liquid contact fraction f_1 should be responsible for such excellent superhydrophobicity.

3.2. Vapor Condensation under Ambient Conditions. Figure 2 showed the time-lapse top-view optical images of dropwise condensation on the horizontally placed superhydrophobic copper surface with sisal-like nanoribbon structures at 90% RH. It can be seen that in over a 1 h experiment, the condensate drops remained spherical and continuously departed from the surface via coalescence with neighboring drops (Figure 2a, the dashed circles). The spontaneous motion frequency of condensate droplets with diameter less than ~7.5 μm (most visible condensate drops were smaller than ~7.5 μm) was as high as 72 drops/s. Figure 2b showed a large drop (diameter ~150 μm) quickly moving from the image left/upper corner to middle location (the dashed circles). The distance was ~450 μm and the time consumed was only ~0.04 s, thus the lateral velocity was approximately 11.25 mm/s. To droplets less than this drop, their velocities should be higher because of their smaller mass.[3]

Figure 3a showed a larger drop (~150 μm) that appeared bright in the middle where light was reflected toward the

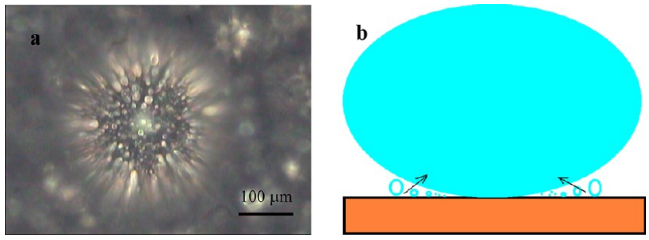

Figure 3. (a) Snapshot (top view) of continuous nucleation, growing, coalescence, departure, and renucleation observed through one larger condensed droplet on superhydrophobic copper surface with sisal-like nanoribbon structures. The temperature of sample surface was 0−1 °C and the environmental RH was 90% (25 °C). The evolution frequency was much higher (up to 132 drops/s) than those observed on area between larger drops. (b) Schematic illustration showing mechanism of even faster spontaneous motion under a larger drop: easier and quick coalescence of condensate droplets to the edge of larger drop bottom. Video S3 is available in the Supporting Information.

microscope objective. Continuous process of nucleation, growing, coalescence, departure, and renucleation with much higher frequency (up to 132 drops/s) than those on area between larger drops (72 drops/s) were found. This should be caused by the much easier and much quicker coalescence of large numbers of condensate droplets between themselves and to the bottom edge of larger drop due to the very narrow space between the larger drop and surface around contact area (Figure 3b).

During the whole condensation process, most self-repelled droplets were smaller than ~7.5 μm in diameter and a few largest ones were ~150 μm. They were all much smaller than the average drop departure size (~300 μm) of condensate droplets on the $Cu(OH)_2$ nanostructured SHS reported by

Dietz et al.,[6] where they placed the surface with a tilt angle of 30° from the horizontal and recorded the dropwise condensation process by a ESEM video at 1 frames/s for 4 min. Similar behavior has been observed before by Narhe et al.[25] and Dorrer et al.[26] This demonstrated that the surface fabricated here may be more effective in improving dropwise condensation.

In addition to at RH 90%, vapor condensation experiments at 30% and 60% RH were also carried out. The corresponding spontaneous motion frequencies of condensed droplets were 3 and 21 drops/s, respectively, both much lower than that at 90% RH (Table 1). These significant decreases should be caused by the much slower nucleation, growing velocity and coalescence probability because of low RH and as well as decreased supercooling extent (dew point ascending along with increase in RH).

Table 1. Spontaneous Motion Frequencies of Condensate Drops As a Function of RH[a]

RH (%) (air temp. 25 °C)	30	60	90
dew point (°C)	6.5	17	23.5
spontaneous motion frequencies (drops/s)	3	21	72

[a]The copper surface was oxidized by immersing in diluted ammonia aqueous solution at ~5 °C for 96 h and then fluorinated for 1 h. The temperature of surface in condensation was 0−1 °C.

Similar condensation experiments were also performed on the superhydrophobic copper surface with defoliation-like nanosheet structures (Figure 4), lotus leaf and butterfly wing (Figure 5). No obvious spontaneous motion of droplets was found on these SHSs even the RH was as high as 90%. Moreover, the droplets were even "adsorbed" into butterfly wing at the late stage of condensation followed by appearing surface feature structures (the dashed circles in Figure 5b). This confirms that not all SHSs supports spontaneous motion of condensate droplets on them. Similar condensation phenomenon on lotus leaf was also reported by Cheng et al.[27] and Chen et al.,[28] where they found that condensate drops tended to stick to the lotus leaf and could be removed only by drops of large size or extra momentum such as mechanical vibration.

After 1 h condensation at 90% RH, little amount of water drops were found on the superhydrophobic copper surface with the sisal-like nanoribbon structures while arrays of glittering and transparent much larger drops (3−5 mm in diameter) were found on the superhydrophobic copper surface with the defoliation-like nanosheet structures (see the Supporting Information, Figure S1). This implies that there are at least two different type of dropwise condensation on SHSs, e.g., "drying" one and "wetting" one.

3.3. Microscopic Mechanism of Spontaneous Motion.

The spontaneous motion is powered by the surface energy released upon drop coalescence.[1−3] However, from more microscopic viewpoint, whether spontaneous motion occurs also depends on the interaction between the droplets and the surface. On the superhydrophobic copper surfaces with the sisal-like nanoribbon structures, the self-repelled droplets (1−150 μm in diameter) were much larger than a single nanoribbon (~200 nm in diameter). Thus the main obstacle to drop motion on the surface arises from contact angle hysteresis that pins the drop edge. The less pinning effect (Jiang et al[16] defined here pinning effect as work of adhesion), the more obvious spontaneous motion phenomenon would be. It is well-known that the Cassie state drops have little pinning effect thus maintaining in the Cassie state is crucial to coalesce-induced spontaneous motion.

At the beginning of nucleation, nucleated droplets must have the radius of curvature, r, greater than the critical radius, $r_{min.}$ Depending on the level of surface subcooling, the value of r_{min} varies from a few nanometers to a few hundred nanometers.[18] At high supersaturation such as 90% RH (room temperature) and 25 k subcooling surface (0−1 °C surface temperature), the critical radius for nucleation may be very small. Thus the nucleation starts to occur on the top, wall and bottom of nanoribbons, disregard the morphology of the nanostructures. At a little late stage, droplets coalescence dominates the drop growth till filling up the gaps between the nanostructures. Then a liquid spot with a relatively flat external surface forms.[15,18,29]

The interface free energy (IFE) of this shaped condensate, however, is high. The upward surface tension force may be larger than the interaction force between the solid surface and condensate water, which is determined by the real contact area between water and nanostructure surface. As a result, the condensate droplet may spontaneously change its shape to reduce the IFE and finally appears a Cassie[29] or a Wenzel−Cassie transition state on the rough surface (Figure 6). When these droplets coalesce, Cassie droplets forms Cassie drops. To the transition drops, the surface energy released upon coalescence of two droplets (10 times larger than the typical energy barrier for Wenzel to Cassie transition[30]) may quickly transfer the merged drops into Cassie ones. It is such an instantaneous Cassie state that caused the drops departed from the surface easily. Nanogaps on the sisal-like nanoribbon structures favor the formation of the above instantaneous Cassie state and thus lead to spontaneous motion phenomenon of condensate microdroplets on them.

On the defoliation-like SHS, both the nanosheet width and space are much smaller than those on the sisal-like SHS. However, the roughness ratio of total surface area in contact

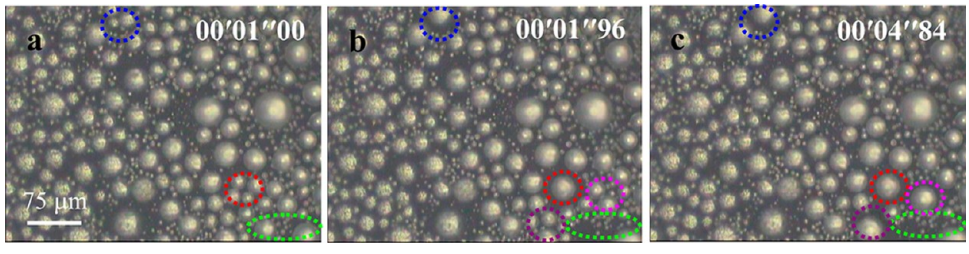

Figure 4. Time-lapse optical images (top-view) of vapor condensation on horizontally placed superhydrophobic copper surface with defoliation-like nanosheet structures. The temperature of sample surface was 0−1 °C and the environmental RH was 90% (25 °C). The spontaneous motion frequency of condensed droplets was only 7 drops/s and the velocity was very limited (mostly was immobilize coalescence).

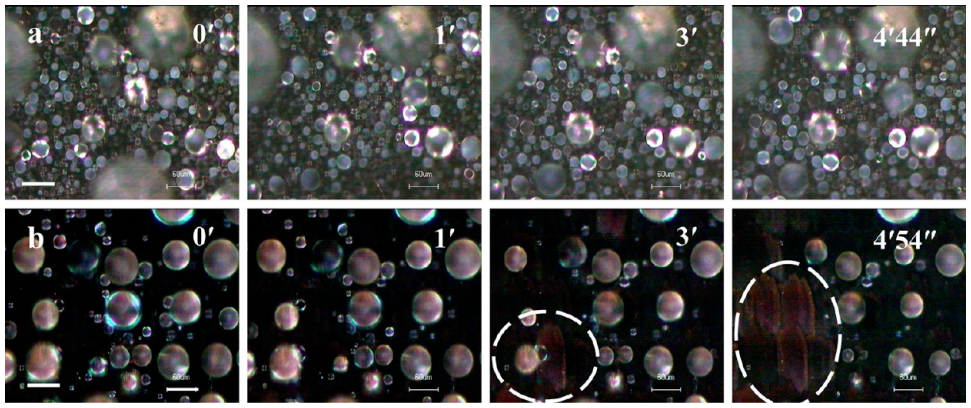

Figure 5. Time-lapse optical images (top-view) of vapor condensation on the horizontally placed (a) lotus leaf and (b) butterfly wing. The temperature of sample surfaces was 0−1 °C and the environmental RH was 90% (25 °C). The scale bar was 60 μm. No obvious spontaneous motion of droplets was found on these two SHSs.

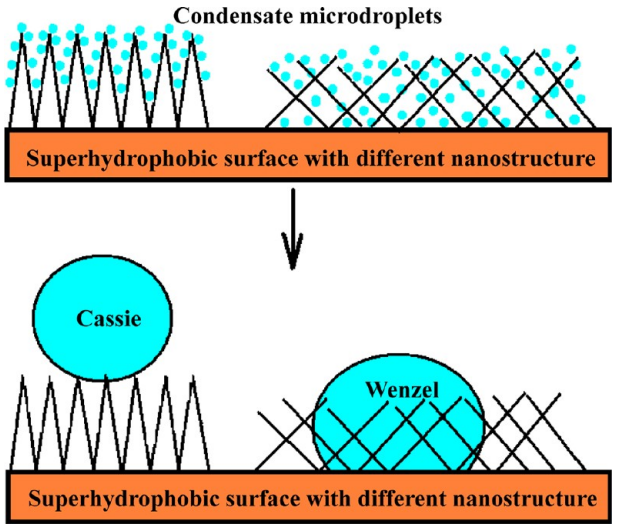

Figure 6. Schematic illustration of vapor condensation and instantaneous Cassie/Wenzel state of droplets on SHSs with different type of nanostructures. The condensate may spontaneously complete Wenzel-to-Cassie transition on the surface with sisal-like nanoribbon structures, whereas it always holds Wenzel state on the surface with defoliation-like nanosheet structures because of different depinning abilities.

with liquid over the projected area in the penetrated Wenzel state, *r*, is higher (∼2.1 calculated from ∼130 °CA at subcooling surface. see Figure 7c, d). More seriously, the oblique nanosheets formed many covered aperture. Vapor can not only condense on the top of nanosheets but also condense within these apertures. The real contact area between condensed water and nanosheet surface was higher thus forms larger pinning effect or energy barrier to microdroplets Wenzel−Cassie transition. As a result, the drops were always remained at Wenzel state (Figure 6). After coalescence, the merged drops are still in Wenzel state. The surface energy released from the reduction of total liquid−air interfacial area of such Wenzel droplets is low while the pinning effect or work of adhesion[16] of the merged Wenzel drops is high. As a result, no spontaneous motion phenomenon was detected on such surfaces. This implies that only SHS with small enough *r* (at least <2.1), a coalescence-triggered self-propelled motion of droplets can occur spontaneously.

The Wenzel−Cassie transition can also be explained by the capillary force generated in the nanogaps. According to the study by Wong et al.,[31] when the vapor condensed in narrow gaps forming by inclined walls, the Laplace pressure is the difference between the pressure on the liquid side of the meniscus and the atmospheric pressure (eq 1).

$$\Delta p = p - p_0 = -\frac{\lambda\cos(\theta - \alpha)}{R_0 + h\tan\alpha} \quad (1)$$

It is factually the upward driving force for Wenzel−Cassie transition and is inversely proportional with the curvature radius of water meniscus in each gap and the solid surface energy. The curvature radius descends significantly with the decrease of inclination angle (α) of wall forming gaps. Thus an acute angle brings larger Laplace pressure than an obtuse angle does. On the sisal-like SHS, the angles formed by two adjacent nanoribbons are much smaller than those formed on the defoliation-like SHS (see Figure 1). As a result, Laplace pressure forming on the sisal-like SHS is larger than that forming on the defoliation-like SHS, and therefore the condensate droplets on the sisal-like SHS tend to be pushed upward.

On the lotus leaf, spontaneous motion is also poor. This should be related to the lower surface energy of the FAS17 coating (the physical contact angle $\theta p = 108° \pm 4°$ compared to the wax coating of lotus leaves $\theta p = 74° \pm 9°$).[32] Factually, when the upward surface tension force pulls up the condensed water spot from the nanogaps, the less interaction force between the solid surface and water, the easier Wenzel−Cassie transition can be completed. Here the interaction force not only depends on the detailed surface nanostructures, but also depends on the chemical aspect of the structure. The lower surface energy, the lower above interaction force would be. Regarding the butterfly wing, the immobile condensate may be caused by the surface special parallel nanostripe structures:[33] when the microdroplets condensed within the nanoslots fill up the slots, the water spot can not easily recede out to the outmost surface to form discrete spherical Cassie droplets due to large resistance caused by long distance interactions between water and solid surface. As a result, no spontaneous motion occurs.

As the droplets during Wenzel-to-Cassie transition are so tiny, it is very difficult to observe them directly even by ESEM.[17,18,34,35] To confirm above hypothesis on the state of

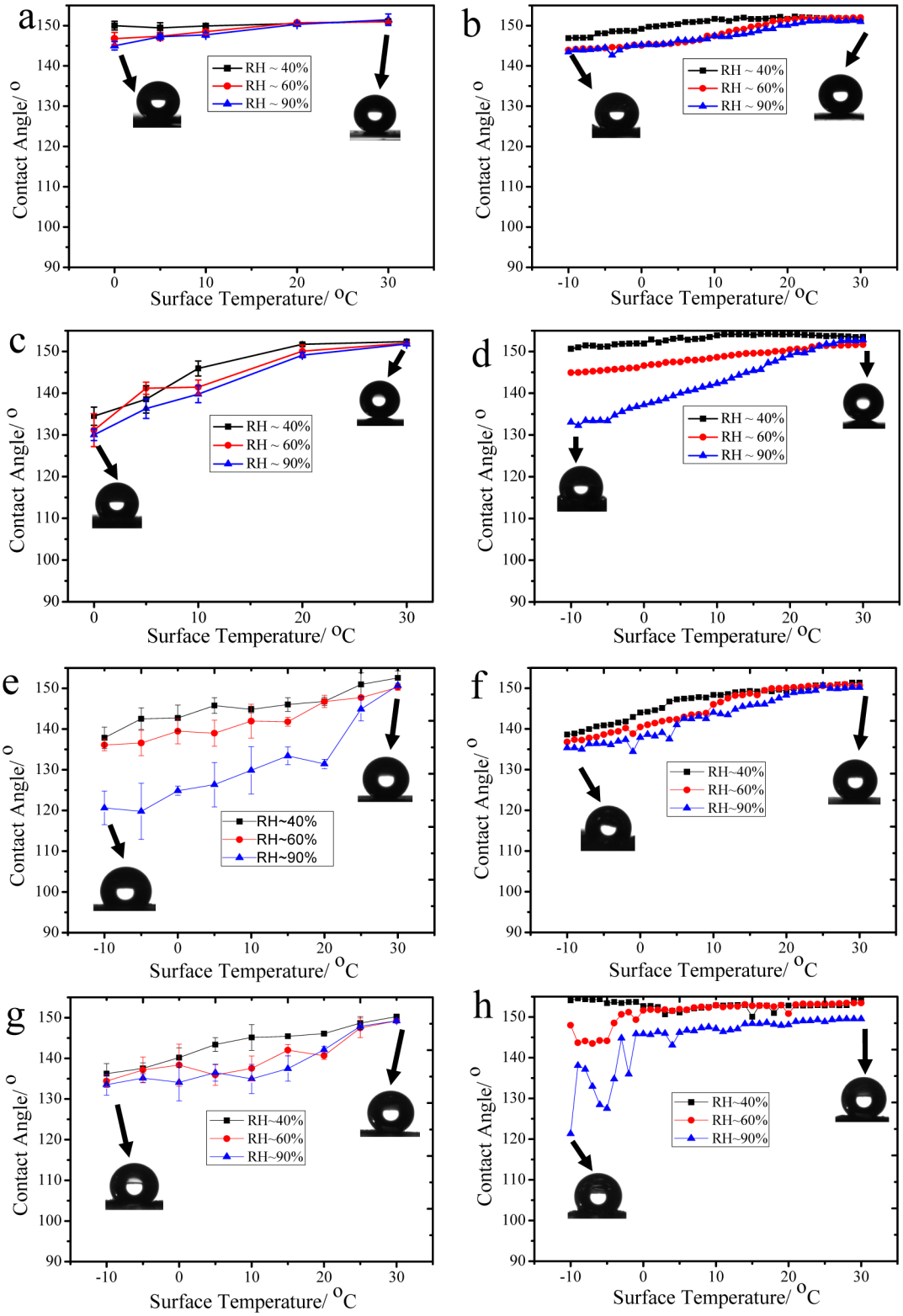

Figure 7. CAs of water drops (a, b) on copper surface with sisal-like nanoribbon structures, (c, d) on copper surface with defoliation-like nanosheet structures, (e, f) on fresh lotus leaf and (g, h) on butterfly wing. a, c, e, and g are static CAs of sessile drops placed on surfaces at different cooling stage and b, d, f, and h are changes of CAs of each sessile drop during the cooling procedure.

condensate droplets (Cassie or Wenzel), the profile change of a sessile water drop under dew condensation at different RH, e.g., the superhydrophobicity stability in condensation, was checked on the SHSs with different structures. Because it was very difficult to splash down a small droplet onto these SHSs (see first part of Results and Discussion). For test convenience, 4 μL (~2−3 mm in diameter) drops were used in superhydrophobicity stability measurements.

Different from the CAs of 0.5−1 μL drops, CAs of 4 μL drops at room temperature were all less than 155°. The static

dx.doi.org/10.1021/am301767k | ACS Appl. Mater. Interfaces 2012, 4, 6618−6625

CAs of sessile drops placed on the SHS at different cooling stages (Figure 7a, c, e, g) and the dynamic changes of CAs of each sessile drop during the whole 10 min cooling procedure (Figure 7b, d, f, h) show a consistent trend of the superhydrophobicity change versus surface type. From Figure 7 a, c, e to g, or b, d, f to h, it can be seen that the superhydrophobicity stability of the surface with the sisal-like nanoribbon structures under dew condensation is much higher than those of the other three surfaces, where the CAs started to decrease significantly in present of condensate droplets (as the surface temperature decreases). Similar increased wettability has also been reported recently by Chen et al. where they attributed such phenomena to the result of an increase in the solid−liquid contact area fraction.[36,37] However, in the microscopic viewpoint, we think herein our significant decrease in CAs (Figure 7c/d, e/f and g/h) should be caused by the coalescence of the larger sessile water drops with the underlying tiny Wenzel-state droplets condensed earlier on the as-measured surfaces (Figure 7c, e, g) or with the Wenzel-state satellite-droplets generated subsequently in the vicinity of each sessile drop (Figure 7d, f, h),[38] whereas the relatively stable CAs (Figure 7a, b) should be caused by the coalescence of the larger sessile drops with the underlying condensate droplets (Figure 7a) or near satellite-droplets (Figure 7b), both in Cassie state.

4. CONCLUSIONS

In this paper, spontaneous motion of condensate drops on different type of SHSs was compared. The microscopic mechanism of spontaneous motion was analyzed in terms of the nanostructure morphology. The results showed that only SHS possessing nanostructures with small enough Wenzel roughness parameter r (at least <2.1) and nanogaps forming high enough Laplace pressure that favors condensate droplets easier Wenzel−Cassie transition. The instantaneous Cassie state of the condensed droplets prior to coalescence plays a key role in coalesced drops departure. This study would be helpful in designing new superhydrophobic surfaces to sustain continuous dropwise condensation, collect condensed water, and engage in anti-icing.

■ ASSOCIATED CONTENT

Supporting Information

Video S1 corresponding to Figure 2a and Video S2 corresponding to Figure 2b recorded the spontaneous motion of condensate drops on SHS with sisal-like nanoribbon structures. Video S3 corresponding to Figure 3 recorded the much faster spontaneous motion of condensate droplets on SHS with sisal-like nanoribbon structures, which was observed through one larger condensed drop. Figure S1 shows the vapor condensation on different type of superhydrophobic surfaces (surface temperature was 0−1 °C) after 1 h at 90% RH (room temperature). This material is available free of charge via the Internet at http://pubs.acs.org/.

■ AUTHOR INFORMATION

Corresponding Author

*E-mail: meshyao@ust.hk (S.Y.); fengjie@zjut.edu.cn (J.F.).

Notes

The authors declare no competing financial interest.

■ ACKNOWLEDGMENTS

We gratefully acknowledge financial support from the Research Grants Council of Hong Kong under General Research Fund 621110, and the National Natural Science Foundation of China (Grant 51172206).

■ REFERENCES

(1) Chen, C. H.; Cai, Q.; Tsai, C.; Chen, C. L.; Xiong, G.; Yu, Y.; Ren, Z. *Appl. Phys. Lett.* **2007**, *90*, 173108−1−173108−3.
(2) Dorrer, C.; Rühe, J. *Adv. Mater.* **2008**, *20*, 159−163.
(3) Boreyko, J. B.; Chen, C. H. *Phys. Rev. Lett.* **2009**, *103*, 184501−1−184501−4.
(4) Chen, X.; Wu, J.; Ma, R.; Hua, M.; Koratkar, N.; Yao, S.; Wang, Z. *Adv. Funct. Mater.* **2011**, *21*, 4617−4623.
(5) Feng, J.; Qin, Z. Q.; Yao, S. H. *Langmuir* **2012**, *28*, 6067−6075.
(6) Dietz, C.; Rykaczewski, K.; Fedorov, A. G.; Joshi, Y. *Appl. Phys. Lett.* **2010**, *97*, 033104−1−033104−4.
(7) Rykaczewski, K.; Scott, J. H. J.; Rajauria, S.; Chinn, J.; Chinn, A. M.; Jones, W. *Soft Matter* **2011**, *7*, 8749−8752.
(8) Miljkovic, N.; Enright, R.; Wang, E. N. *ACS Nano* **2012**, *6*, 1776−1785.
(9) Zheng, Y. M.; Bai, H.; Huang, Z. B.; Tian, X. L.; Nie, F. Q.; Zhao, Y.; Zhai, J.; Jiang, L. *Nature* **2010**, *463*, 640−643.
(10) Thickett, S. C.; Neto, C.; Harris, A. T. *Adv. Mater.* **2011**, *23*, 3718−3722.
(11) Kulinich, S. A.; Farhadi, S.; Nose, K.; Du, X. W. *Langmuir* **2011**, *27*, 25−29.
(12) Varanasi, K. K.; Deng, T.; Smith, J. D.; Hsu, M.; Bhate, N. *Appl. Phys. Lett.* **2010**, *97*, 234102−1−234102−3.
(13) Narhe, R. D.; Gonzalez-Vinas, W.; Beysens, D. A. *Appl. Surf. Sci.* **2010**, *256*, 4930−4933.
(14) Wang, P.; Zhang, D.; Qiu, R. *Corros. Sci.* **2012**, *54*, 77−84.
(15) Liu, T. Q.; Sun, W.; Sun, X. Y.; Ai, H. R. *Colloids Surf., A* **2012**, *414*, 366−374.
(16) He, M.; Zhou, X.; Zeng, X.; Cui, D.; Zhang, L.; Chen, J.; Li, H.; Wang, J.; Cao, Z.; Song, L.; Jiang, L. *Soft Matter* **2012**, *8*, 6680−6683.
(17) Rykaczewski, K. *Langmuir* **2012**, *28*, 7720−7729.
(18) Rykaczewski, K.; Osborn, W. A.; Chinn, J.; Walker, M. L.; Scott, J. H. J.; Jones, W.; Hao, C.; Yao, S.; Wang, Z. *Soft Matter* **2012**, *8*, 8786−8794.
(19) Enright, R.; Miljkovic, N.; Al-Obeid, A.; Thompson, C. V.; Wang, E. N. *Langmuir* **2012**, *28*, 14424−14432.
(20) Wen, X.; Xie, Y.; Choi, C. L.; Wan, K. C.; Li, X. Y.; Yang, S. *Langmuir* **2005**, *21*, 4729−4737.
(21) Yao, X.; Chen, Q.; Xu, L.; Li, Q.; Song, Y.; Gao, X.; Quéré, D.; Jiang, L. *Adv. Funct. Mater.* **2010**, *20*, 656−662.
(22) Zhang, Y. F.; Yu, X. Q.; Zhou, Q. H.; Chen, F.; Kang, K. N. *Appl. Surf. Sci.* **2010**, *256*, 1883−1887.
(23) Zhang, X.; Guo, Y. G.; Zhang, P. Y.; Wu, Z. S.; Zhang, Z. J. *Mater. Lett.* **2010**, *64*, 1200−1203.
(24) Zhang, X.; Shi, F.; Yu, X.; Liu, H.; Fu, Y.; Wang, Z. Q.; Jiang, L.; Li, X. Y. *J. Am. Chem. Soc.* **2004**, *126*, 3064−3065.
(25) Narhe, R. D.; Beysens, D. A. *Langmuir* **2007**, *23*, 6486−6489.
(26) Dorrer, C.; Ruhe, J. *Langmuir* **2007**, *23*, 3820−3824.
(27) Cheng, Y. T.; Rodak, D. E. *Appl. Phys. Lett.* **2005**, *86*, 144101−1−144101−3.
(28) Boreyko, J. B.; Chen, C. H. *Phys. Rev. Lett.* **2009**, *103*, 174502−1−174502−4.
(29) Liu, T.; Sun, W.; Sun, X.; Ai, H. *Langmuir* **2010**, *26*, 14835−14841.
(30) Ishino, C.; Okumura, K.; Quere, D. *Europhys. Lett.* **2004**, *68*, 419−425.
(31) Xiu, Y.; Zhu, L.; Hess, D. W.; Wong, C. P. *Nano Lett.* **2007**, *7*, 3388−3393.
(32) Cheng, Y. T.; Rodak, D. E.; Wong, C. A.; Hayden, C. A. *Nanotechnology* **2006**, *17*, 1359−1362.
(33) Zheng, Y. M.; Gao, X. F.; Jiang, L. *Soft Matter* **2007**, *3*, 178−182.
(34) Rykaczewski, K.; Scott., J. H. J. *ACS Nano* **2011**, *5*, 5962−5968.

(35) Rykaczewski, K.; Scott, J. H. J.; Fedorov, A. G. *Appl. Phys. Lett.* **2011**, *98*, 093106−1−093106−3.
(36) Yin, L.; Zhu, L.; Wang, Q.; Ding, J.; Chen, Q. *ACS Appl. Mater. Interfaces* **2011**, *3*, 1254−1260.
(37) Yin, L.; Wang, Y.; Ding, J.; Wang, Q.; Chen, Q. *Appl. Surf. Sci.* **2012**, *258*, 4063−4068.
(38) Mockenhaupt, B.; Ensikat, H. J.; Spaeth, M.; Barthlott, W. *Langmuir* **2008**, *24*, 13591−13597.